High-speed atomic force microscopy on soft matter

École Polytechnique Fédérale de Lausanne
Lawrence National Berkeley Laboratory

Master's thesis by Arnaud Bénard

Supervisors:
Prof. Philippe Renaud, EPFL
Dr. Paul Ashby, LBNL
Dr. Dominik Ziegler, LBNL

Master Thesis: Arnaud Bénard
High-speed atomic force microscopy on soft matter

Molecular Foundry, Lawrence Berkeley National Laboratory, Berkeley, California, USA.

In cooperation with: EPFL-STI-IMT-LMIS4, Microsystems Laboratory 4, EPFL Lausanne, Switzerland

Project Description:

The ability of atomic force microscopy (AFM) to achieve atomic resolution made it one of the most important tools for nanoscience. But piezo-based scanning and serial data collection from the local probe makes image collection slow and unable to match the timescales of many dynamic processes. To overcome this problem we are using advanced scan algorithms such as spiral and cyclic scanning or boundary tracking to increase temporal resolution compared to slow raster scanning techniques. Spiral scanning better matches the mechanical limitations of the AFM scanner and allows higher tip velocities without distorting the image, and using image processing techniques such as inpainting high-resolution images can be restored from sparse quickly collected images without applying more force or increasing bandwidth.

The objective of this master thesis is to achieve video rate imaging using commercially available piezo scanners while maintaining sub-nanometer resolution. To this end already implemented scan patterns need to be improved as follows, the execution time of current inpainting algorithms need to be shortened (processing on the graphics processor), and the noise in the position sensor data is to be reduced using intelligent filter design (Kalman filtering). The fast scan algorithms are to be tested in combination with our newly developed encased cantilevers. The encasement of these cantilevers keeps the resonator dry and only the sharp tip interacts with the sample. This maintains low damping and high resonance frequency as operating in air, which results in increased force sensitivity and allows higher scan speeds operating in liquids. The combination of these cantilevers with fast scan algorithms is believed to enable capturing dynamics of soft samples without perturbing the system under observation. A variety of relevant samples ranging from suspended lipid bilayers, collagen, crystal growth, polymer blends, or membrane proteins in living cells are to be considered.

The results should be thoroughly prepared so that they can be easily incorporated into a manuscript to be submitted to well-known peer-review journals.

The Molecular Foundry

The master thesis will be performed at the Molecular Foundry, in the Lawrence Berkeley National Laboratory, Berkeley, California USA. (http://foundry.lbl.gov/). The Molecular Foundry is a US Department of Energy funded institution, providing support to researchers from around the world whose work can benefit from or contribute to nanoscience. The Foundry's research program is centered around four interdisciplinary themes: Combinatorial Nanoscience; Nanointerfaces; Multimodal in situ Nanoimaging; and Single-Digit Nanofabrication. The six in-house research facilities provide state-of-the-art instruments, materials, technical expertise and training to fulfill all tasks involved in this master thesis.

Tasks and Objectives:

- Literature research on fast scanning AFMs techniques.
- Familiarize with existing scan algorithms implemented for on existing home build and Asylum (MFP-3D) microscopes.
- Quantify the performance of existing algorithms in terms of scan-speed, quality of images.
- Improve in-painting techniques (by using OpenGL for instance)
- Implement Kalman filtering on the sensor data
- Test scan algorithms on relevant dynamic samples.
- Preparation of the results for presentation and composition of a report.

Literature:

A collection of high-speed AFM data can be found at
http://www.highspeedscanning.com/high-speed-afm-gallery.html

Ando, T., Uchihashi, T., & Fukuma, T., (2008). High-speed atomic force microscopy for nano-visualization of dynamic biomolecular processes. Progress in Surface Science, 83(7-9), 337-437.

Yong, Y. K., Moheimani, S. O. & Petersen, I. R. (2010). High-speed cycloid-scan atomic force microscopy. Nanotechnology, 21(36), 365503.

Mahmood, I. A., & Reza Moheimani, S. O. (2009). Fast spiral-scan atomic force microscopy. Nanotechnology, 20(36), 365503.

Meyer T., et al., Fast Atomic Force Microscopy Imaging using Self-Intersecting Scans and Inpainting, in preparation.
www.csulb.edu/~jchang9/files/AFM_UCLA_REU_2011.pdf
www.csulb.edu/~jchang9/files/toward_capturing_soft_molecular_material_dynamics.pdf

Project Start: (To be discussed) July, 2012.
Project End: 6 month from starting date

Project Supervisor:
Prof. Dr. Philippe Renaud (philippe.renaud@epfl.ch, Phone: +41-21-693-2596)
Microsystems Laboratory 4, EPFL-STI-IMT-LMIS4, Station 17, CH-1015 Switzerland.

Project Advisors:
Dr. Dominik Ziegler (dziegler@lbl.gov, Phone: +1-510-486-7347, Building 67 Room 1202)
and Dr. Paul Ashby (pdashby@lbl.gov, Phone: +1-510-486-7081, Building 67 Room 2228)
Materials Sciences Division, Mail Stop 67R2206, Lawrence Berkeley National Laboratory,
1 Cyclotron Road, Berkeley, California 94720, USA.

Berkeley, December 21st 2011.

LMIS4 Résumé de Travail pratique de Master 15/03/13

High-speed atomic force microscopy on soft matter

Arnaud Benard, Section Microtechnique

Assistant: *Dominik Ziegler, Paul Ashby*

Professeur: *Philippe Renaud*

Summary of the project

The principle of an AFM is to sense forces between a sharp tip and a surface. Since its invention in 1986, multiple improvements have allowed this technology to operate at higher speed and on larger surfaces. Still, the bulky mechanic of the AFM, which is managed by position controllers on the three axis, leads to errors caused by creep, drift and hysteresis.

Instead of using controllers on the horizontal plane (X, Y), we simply record the position of the tip with inductive sensors. With this method (open loop), we are not limited to raster scanning (sawtooth) anymore. Indeed, we can scan the sample with any pattern (i.e. Archimedean spiral).

Moreover, we have developed a dual actuactors feedback system on the z-axis. This high bandwidth piezoelectric ceramic is implemented on top of the X-Y scanner. This scheme allows the tip to pick up abrupt changes in the topography (high frequency).

Also, we have programmed a method to detect and dynamically correct the tilt on a sample. This technique measures the general topography of the surface and generates a correction signal for the z scanner. The slow z-axis (z scanner) compensates the tilt and takes a load off the fast piezoelectical ceramic.

With spiral scanning, our sparse data is not directly transposed on a grid ; therefore, new tools are needed to generate high quality images. We have programmed an image processing algorithm that uses heat equations inpaiting. We have discussed rendering with Open Graphics Library (OpenGL) and implemented the immediate mode and Vertex Buffer Objects. The latter method renders 100,000 points in 247.9ms at 130 frames per second.

Finally, we have tested our setup with two experiments. The first one involved scanning a calibration grating with Achimedean spirals and proved that our tilt correction algorithm worked successfully.

The second one measured the dissolution of calcite in water. We have achieved high speed scans and successfully imaged the latter process.

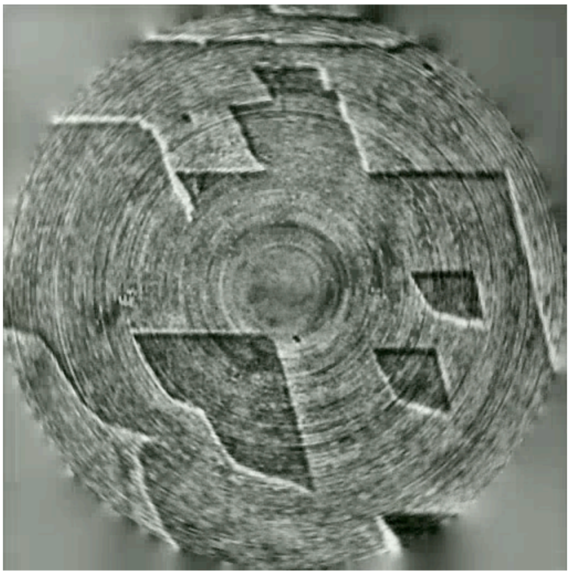

Calcite dissolution (5s per frame, 100 loops, 5µm)

Contents

List of Figures

List of Tables

1 Introduction

In 1986, a group of scientists from IBM research developed the first Atomic Force Microscope.[3] The original idea was to sense forces between a sharp tip and a surface. The deflection of the cantilever is measured using a laser reflected from the top of the cantilever into a photodetector(array of photodiodes). Nowadays, AFM's applications range from measuring elastic properties of biological samples to imaging of surface topography[4] [5]. The former technique is achieved by using a XY-scanner to move the sample on the horizontal plane. Therefore, the AFM acquires data on different points of the surface. Additionally, AFMs have a feedback system to maintain a constant tip-sample force.

The most conventional way to scan is with a raster pattern (sawtooth). This technique steers the tip of the AFM on specific points of a grid. Past AFM research has been focused on improving position controllers. Indeed, the AFM precision depends on the quality of the closed loop feedback. These improvements, however, didn't solve fundamental problems with raster scanning. Most of the data is thrown away (trace and retrace) and the actual position on the XY plane is inaccurate - and directly correlated with the efficiency of the position controller. Because of its limited bandwidth, fast raster scans generate distortions in the image.[6]

Spiral pattern techniques generate high-quality images at higher scan frequencies than the raster one. [7]. Also, this method reduces the number of data points necessary. [8]We need, however, needs new techniques to render images. Fortunately, image processing algorithms like inpainting [9] or Delaunay triangulation have been developed to generate images from sparse data.[8].

The bandwidth on the z-axis control loop is limited by the dynamics of the z scanner.[10]. One way to improve the AFM feedback loop is implementing model based controllers or high frequency actuators [11]. The drawback with these actuators is the decrease in the positioning range. We can achieve higher frequencies by using a small piezoelectric ceramic.[11]

In this thesis, we will see how we can use non-raster scan patterns to improve the bandwidth on the XY-plane. Also, we have developed image processing algorithms to render non-gridded data. We use the popular Open Graphics Library (OpenGL) for the rendering of the X, Y, Z data and investigate ways to use the Graphics Processing Unit (GPU) to improve the computing time.

We will implement new ways to go beyond the limitations on the z-axis with tilt correction and dual actuators feedback. If an image is tilted, you can use first-order plane fitting to correct the image. A more efficient way is to dynamically compensate for the tilt of the sample. Finally, we will see how to improve the bandwidth on the z-axis by introducing a small piezoelectric ceramics.

2 Visualization of non-gridded data

Current AFMs use position controllers on the XY axis to steer the tip at a specific position on the sample. The controller uses the position sensors to measure the error with the ideal position (PID). Then, it will force the tip to move at the corrected spot. Instead of using this method, we work in open loop and only register the data of the position sensors. We don't try to adjust the position of the tip. We let it move freely and embrace its inaccuracy. One of the advantages of using this method is that we don't need any feedback system on X,Y and the precision of our system is greatly improved. Our current setup (Asylum Research MFP3D) uses inductive sensors(figure 2.1).

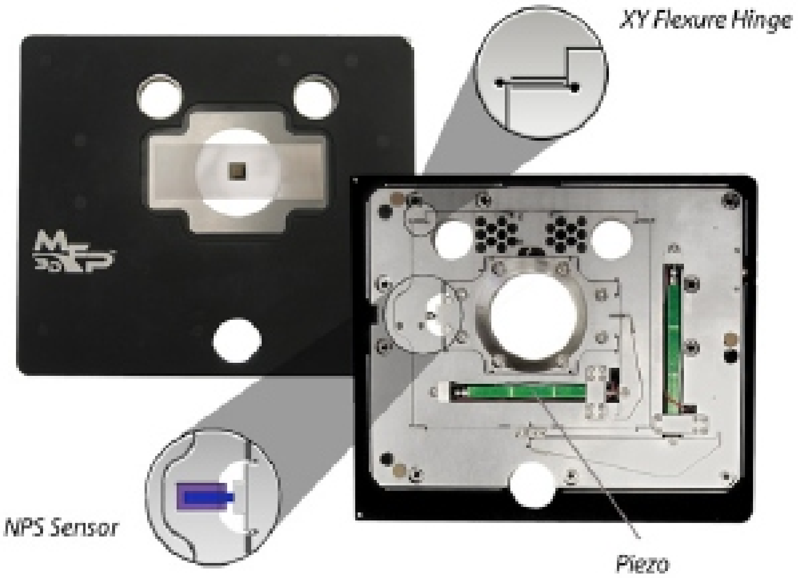

Figure 2.1: The XY scanner uses inductive sensors that measure the exact position of each axis. [1]

Using this technique frees us from raster scan and allows us to explore new patterns (spiral). Because our data is not directly transposed on a grid anymore, image processing algorithms are needed to render our scan. We will see in the next section methods to generate high-quality images from AFM's data.

2.1 Image rendering techniques

We are going to investigate the two following techniques: inpainting and OpenGL. The inpainting methods have been designed and implemented on Matlab by the Paul Ashby Group at LBNL in collaboration with Prof. A. Bertozzi of UCLA. Then, we will discuss using OpenGL for the rendering. We will see different methods to implement this library and benchmark its performance.

2.1.1 Inpainting algorithms

Reconstructing missing parts of images was first developed for restoring photographs and paintings. In the past, the art of restoration was performed manually. Nowadays, similar modern tools like Photoshop or Gimp are used in our mass media.[9].

This process is called inpainting. The principle is to fill a patch with the information of its surroundings. Mathematicians have developed a wide range of algorithms to solve that problem. We will investigate inpainting based on a special case of partial differential equations (PDE) called heat equations.

The heat equation is a PDE that represents the distribution of heat in a region over time.

$$\frac{\partial u}{\partial t} - \alpha \nabla^2 u = 0 \tag{2.1}$$

Where α is the thermal diffusivity - that is interpreted as a "thermal inertia modulus" - and u is the temperature over space and time (i.e. $u(x, y, z, t)$). A high thermal diffusivity implies that the heat moves rapidly.

This algorithm will spread out the information of each point onto missing parts of our grid.

Literature shows that heat equations are powerful enough to fill out these patches of missing data, but they smooth sharp edges(high frequency data)[12]. Indeed, the effect is that these edges are blurred out by the algorithm. Applications of this algorithm are shown in the chapter 4.

2.1.2 OpenGL

In this section, we will see how to render images with OpenGL(Open Graphics Library). It is an API (Application Programming Interface) developed by Silicon Graphics to hide the complexities of interfacing with different 3D accelerators and is mainly used for 3D modeling in video games and simulations. OpenGL leverages the fact that GPUs are designed to render triangles.

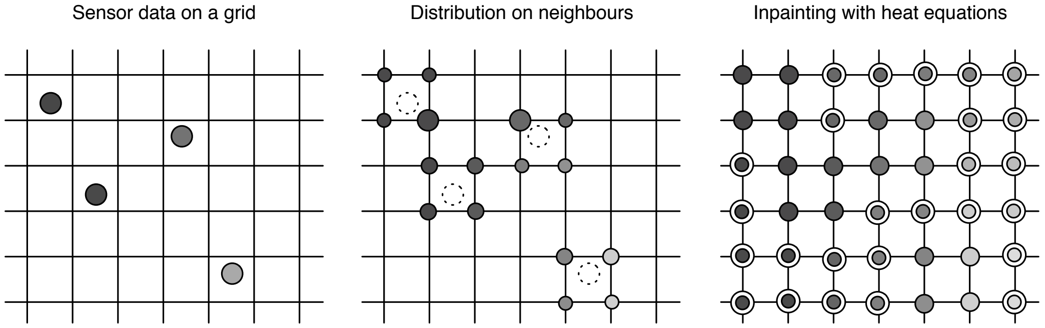

Figure 2.2: The first image shows that we don't have enough informations to fill out all the pixels. We need to project the data onto the neighbors. Finally, the heat equation inpainting will spread the weighted data onto the missing spots.

Indeed, it optimizes the rendering by finding repetition of geometric shapes (tessellation) in the data. The more complex the shape the harder it will be for the GPU to process it. If we already pre-process the data into triangles, we minimize processing costs. [13]

We have designed a program that takes into account the preprocessing of the data. Most of the time, this data will be the information of the topography of the surface (X,Y,Z axis). The flow of our program is described by the figure 2.3. First, we take the X, Y, Z data and generate a list of triplets of points (triangles). Then, we render this list with one of the two following methods: immediate mode and Vertex Buffer Objects.

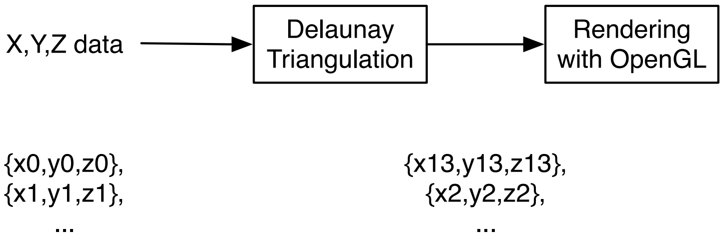

Figure 2.3: Workflow of the rendering program.

Triangulation with Delaunay

The first problem is generating triangles from sparse data. Indeed, OpenGL can only render triangles from a triplet of points. If we render the X, Y, Z data without preprocessing, OpenGL will generate triplets from the closest index in the list. We need efficient algorithms like Delaunay triangulation to take into account the X, Y position of the point and not the index.

The algorithm minimizes the angles of each triangle. The triangulation is successful if no vertex (i.e. 3-dimensional point) is inside a triangle.

Jonathan Shewchuk [14] has developed a library, triangle.c, to compute Delaunay triangulations and other meshes. The Figure 2.4 shows the effect of the program on a spiral scan, which will be discussed later.

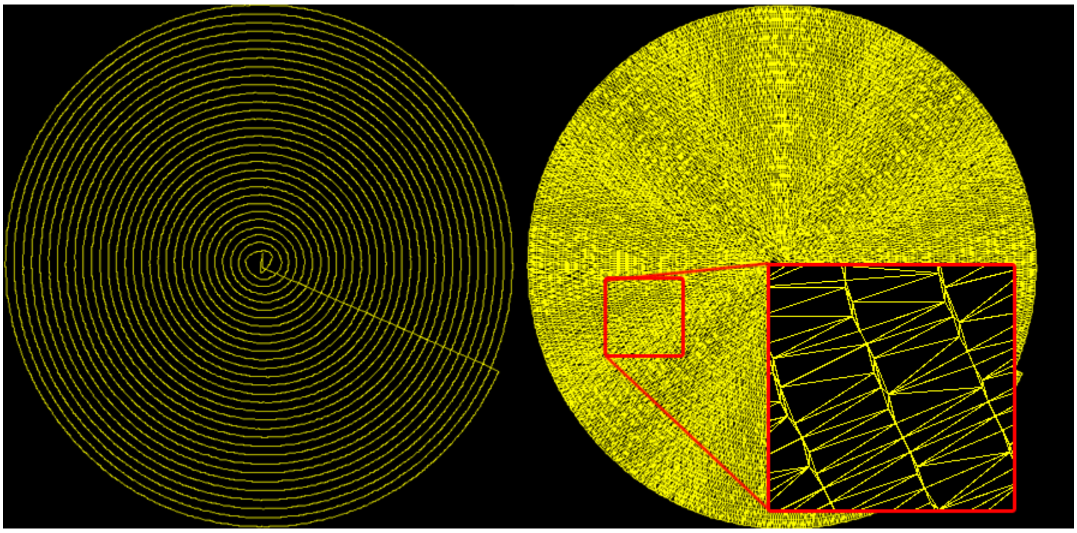

Figure 2.4: Before and after triangulation. This image is rendered by using the triangle.c library. The input data has 20,000 points and the program generates 38,784 triangles.

With this method we can connect the points on a 2D plane. In the figure 2.5, we use the z-axis data to compute the height of each point and render 3D models of our scans. To add colors to our data, OpenGL will create a linear gradient between each of the data points.

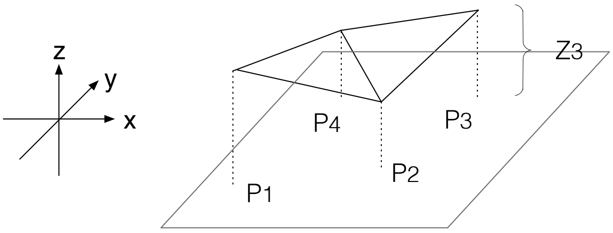

Figure 2.5: Delaunay triangulation: From 2D to 3D

Immediate mode vs Vertex Buffer Objects

The immediate mode is the simplest implementation of OpenGL. Indeed, we render every frame. Action like rotation, translation or resizing of the model will trigger a new frame generation. During this process, the program uploads the vertices to the graphic processing unit(GPU). The power of the immediate mode is its simple implementation (no initialization and extra code). Moreover, it is easier to debug. For a small number of vertices (< 10,000) the immediate mode is appropriate. [15] The problem with this method is that the program doesn't "remember" the data. For instance, a simple rotation shouldn't regenerate a frame but simply perform a change in the point of view.

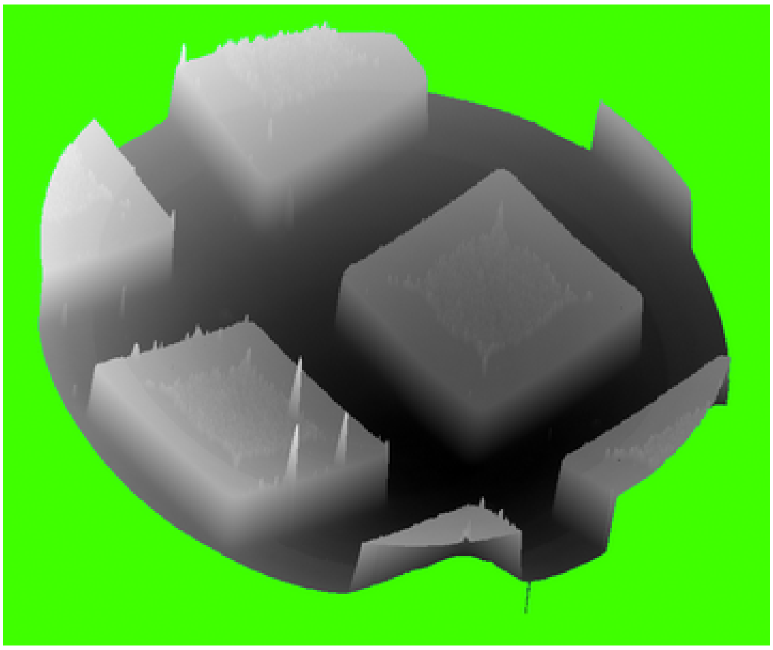

Figure 2.6: OpenGL 3D rendering(1.2M points) of a calibration grating using spiral scans.

If we try to display a significant number of triangles (> 10,000 vertices), the CPU will be the bottleneck. The GPU doesn't start rendering data before the last callback. Thus, the CPU is spoon-feeding the GPU by transferring the data triangle by triangle. Moreover, the number of API calls is proportional to the number of triangles. For instance, if you have 10 triangles you will make $(10*(2+3+3))$ 80 API calls [16]. In conclusion, if you want to render less than 10,000 vertices and are not planning to make a lot of changes in your rendering, the immediate mode is ideal.

One of the problems with the immediate mode is the transfer from the system memory to the GPU. With 10,000 points we can only have 3 frames per second which means that our computer takes 300 ms for the whole process.

Instead of transferring the data from the memory to the GPU, the GPU could read the memory of the program stack. Buffer objects have been created to allow the GPU to have access to that memory. A buffer object is a contiguous untyped memory which the CPU and the GPU both have access to. The process of reading the memory from the GPU is called Direct Memory Access (DMA).

Unfortunately, we can't just upload our data into the memory without any preparation. We need to map the data and make it readable for the GPU which makes the implementation more complex.

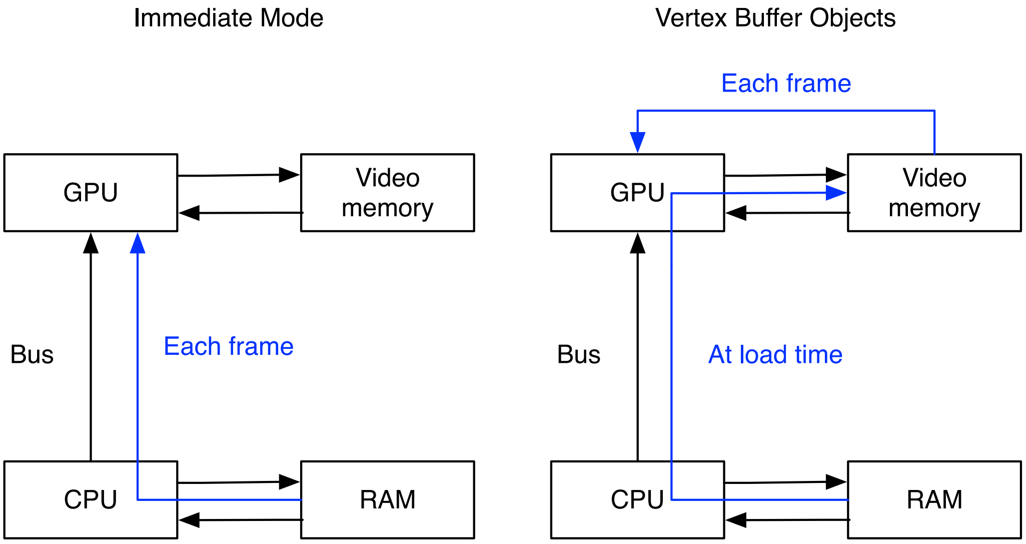

Figure 2.7: Workflow of the immediate mode and the vertex buffer objects[2]

The advantage of this implementation is that you directly pull your data to a shared memory between the CPU and the GPU. Your CPU will spend less cycles making API calls thus improving the performance of the program. The power of the VBOs is that you just need to upload your data and your display function will just bind the VBO. In the figure 2.7, we see the GPU has direct access to our data resulting. Our performance has improved from 3 frames per seconds (FPS) to 130FPS (100,000 points).

The table 2.1 shows the non-linearity of our implementation. We see that Delaunay triangulation doesn't scale well for 1,000,000 points. In AFM scans we will rarely sample 1,000,000 datapoints. The limits of our AFM is 100,000 kHz. If we take 10 second scans at the limit rate, we observe that the computation time is still way below the scanning time.

Table 2.1: Rendering results[ms]

Nb of points	Delaunay	VBO	Total time
1000	2.9	23.9	26.8
10000	8.1	27	35.1
100000	66.9	181	247.9
1000000	640.7	267	907.7

3 Techniques for fast z feedback

Past research has introduced an external piezoelectrical actuator on top of the cantilever to improve the bandwidth and the scan range. drawback with these actuators is the decrease in the positioning range. We can achieve higher frequencies by using a small piezoelectric ceramic.[11] With this scheme, we can combine the advantages of a high bandwidth from the piezoelectrical actuator and the long range of the tip. We are going to put the high bandwidth actuator on top of the X,Y scanner.

3.1 Dual actuators system

The principal feature of an AFM is its probing system. The feedback control system is designed to adjust the motion of the tip on the z-axis. It will adjust the tip-to-sample distance.

The figure 3.1 shows the most classic feedback loop in an AFM. The reference of the controller is the force setpoint. The output of the controller is the topography of our surface. Also, the error signal is the sum between the reference and the deflection of the cantilever.

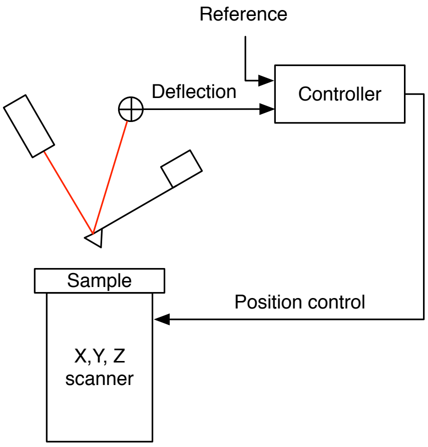

Figure 3.1: Normal AFM setup

The problem with this system is that it can't pick up abrupt changes in the topography.[10] The bandwidth of the cantilever is not large enough. We could use a cantilever with a higher bandwidth, but the amplitude would be too small. We decided to take to the best of both systems and design a dual-actuator system. We use a standard cantilever to scan the surface and we will add a small piezoelectrical ceramic on top of the X-Y scanner. It enables the AFM to have a larger bandwidth thus allowing it to pick up high spatial frequency topography.

We design another feedback system in order to make the X,Y,Z scanner and the piezoelectrical ceramic work together. [17]

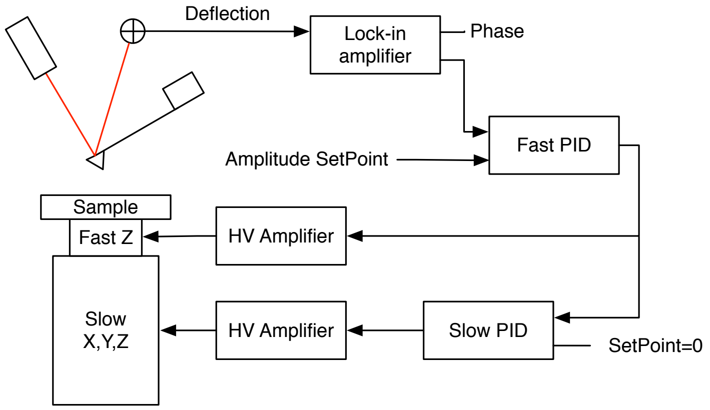

Figure 3.2: Z-feedback using fast and slow piezos.

We need a high-voltage amplifier to operate the small piezoelectric device.

3.2 Tilt compensation

In theory, the mounted sample should be parallel to the XY-Scanner. If the probe/sample angle is not perpendicular, we observe a tilt on the surface. This tilt is problematic when it becomes larger than the features. There are multiple ways to compensate for this. The most common technique is to use post-processing to adjust the image. Flattening algorithms or first-order planefitting restore the image and put the data on the same level. This technique works if the range of the tip is large enough. We have decided to take another approach and dynamically compensate for the tilt. Before performing our scan, we will do a first scan to compute the tilt of the sample by considering our tilt as a 3D plane. Then, we'll generate a tilt correction signal that will be added to the z scanner.

We use a circle pattern to scan the surface of the sample. The radius of the circle is equal to the scan size. It gives us information about the general topography of the surface. Then, we compute the plane equation of the surface by applying a fit in Igor Pro. This fit will generate a plane that models the tilted surface. The input of this fit is the theoretical X-Y output waves of the circle pattern: a sine and a cosine. The data on the z axis is the height.

$$z = a_1 x + a_2 y + a_3 \tag{3.1}$$

The coefficients are computed by minimizing the values of Chi-Square (error function). Then, we generate the waves to send to the controller with the equation ref.

$$wavetosend = a_1 wavex + a_2 wavey \tag{3.2}$$

Wavex and wavey are the output of our scan pattern. With this method, we can do a tilt correction with any scan pattern.

Then, we send the previously computed wave to the controller.

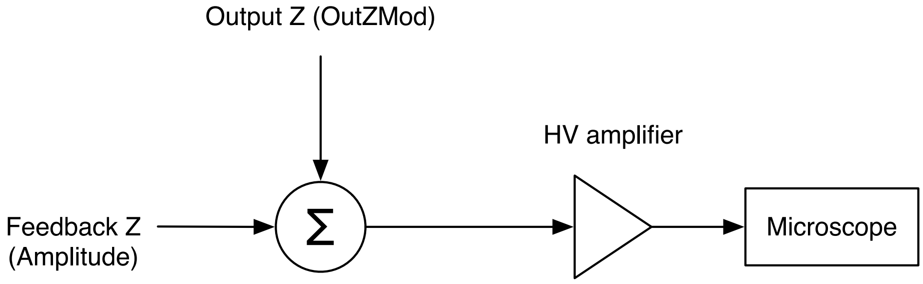

Figure 3.3: Asylum

4 Results

4.1 Calcite experiment

In this experiment we will observe the dissolution of calcite ($CaCO_3$) with water. We have decided to choose this reaction because the chemical reaction leading to the dissolution is simple. Moreover, it is an abundant and geologically important material.[18][19] [20]

The figure 4.1 shows the tilted shape of calcite during dissolution. One part has an angle of 78° and the other 102°[21] [22].

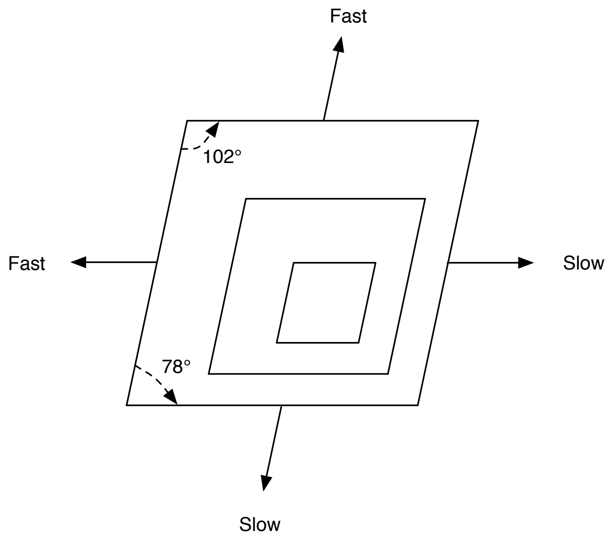

Figure 4.1: Calcite geometry

We have used our dual actuators feedback system with a Budget Sensor Tap150-G cantilever. Calcite dissolution is an interesting process to observe with a high speed AFM.

$$CaCO_3(calcite) + H_20 \rightarrow Ca^{2+} + HCO_3^- + OH^- \tag{4.1}$$

We have mounted our calcite sample on top of the fast piezoelectrical ceramics. Also, we have stuck a plastic cover underneath the piezo for the water. THe calcite will dissolve itself with the pattern shown on figure 4.1. It is linked to its original geometry.

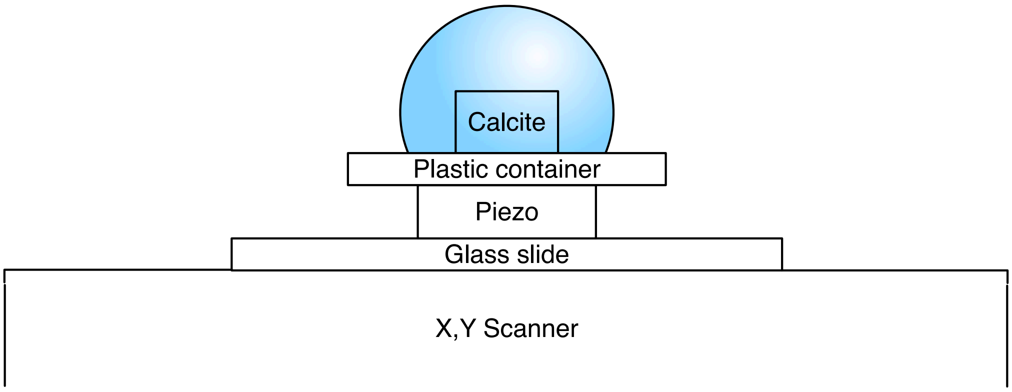

Figure 4.2: Setup for the calcite experiment

We have imaged the same sample with different parameters including scan size, number of spirals and scanning time.

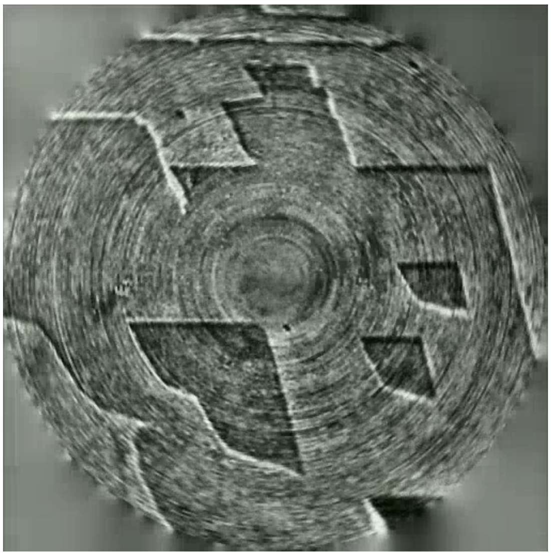

Figure 4.3: 5s per frame / 100 loops / 5 μm

The figure 4.4 shows the evolution of the calcite. Every scan took 10 seconds over a surface of 10 μm. The scan pattern is an Archimidean spiral with 50 loops and is rendered with heat equation inpainting. We observe the evolution of the front wave over time. After a dozen of minutes, the water will saturate the calcite and the reaction will stop. You can redo the experiment by removing the water and adding fresh water afterwards.

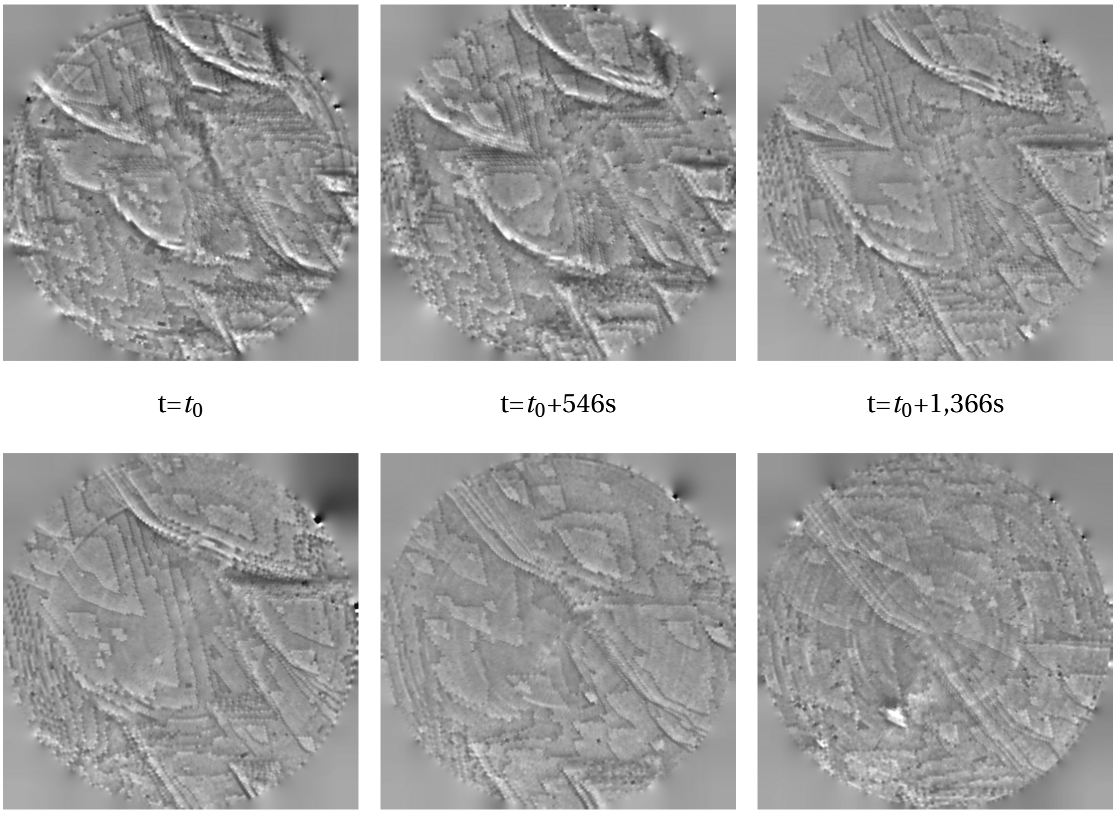

t=t_0 t=t_0+546s t=t_0+1,366s

t=t_0+2200s t=t_0+3404s t=t_0+5148s

Figure 4.4: Evolution of the calcite dissolution over time. 10 μm scan size and 50 loops.

4.2 Tilt correction

In this experiment, we will show the efficiency of the tilt correction. Our sample is a calibration grating with pyramidal features. We use the dual actuators feedback control described in the section 3.1. Also, the scan pattern is an Archimedean spiral, with a radius of 30 μm and 80 loops, described by the equations 4.2.

$$x(t) = \alpha\sqrt{t}cos(\beta\sqrt{t}) \qquad y(t) = \alpha\sqrt{t}sin(\beta\sqrt{t}) \tag{4.2}$$

Before applying the tilt correction, we see on the figure 4.5 a) that our fast piezoelectrical ceramic is saturating. We definitely need to take a load off the actuator.

We have seen in the section 3.2 (equation 3.2) that we need to sample the topography of the surface to compute the plane coefficients. We put a high integral gain for the slow piezo to get the general topography of the sample. The figure 4.5 b) shows that the surface is not perfectly flat (see z-axis).

Then we compute our fitting algorithm on the x,y and z data of the figure 4.5 b).

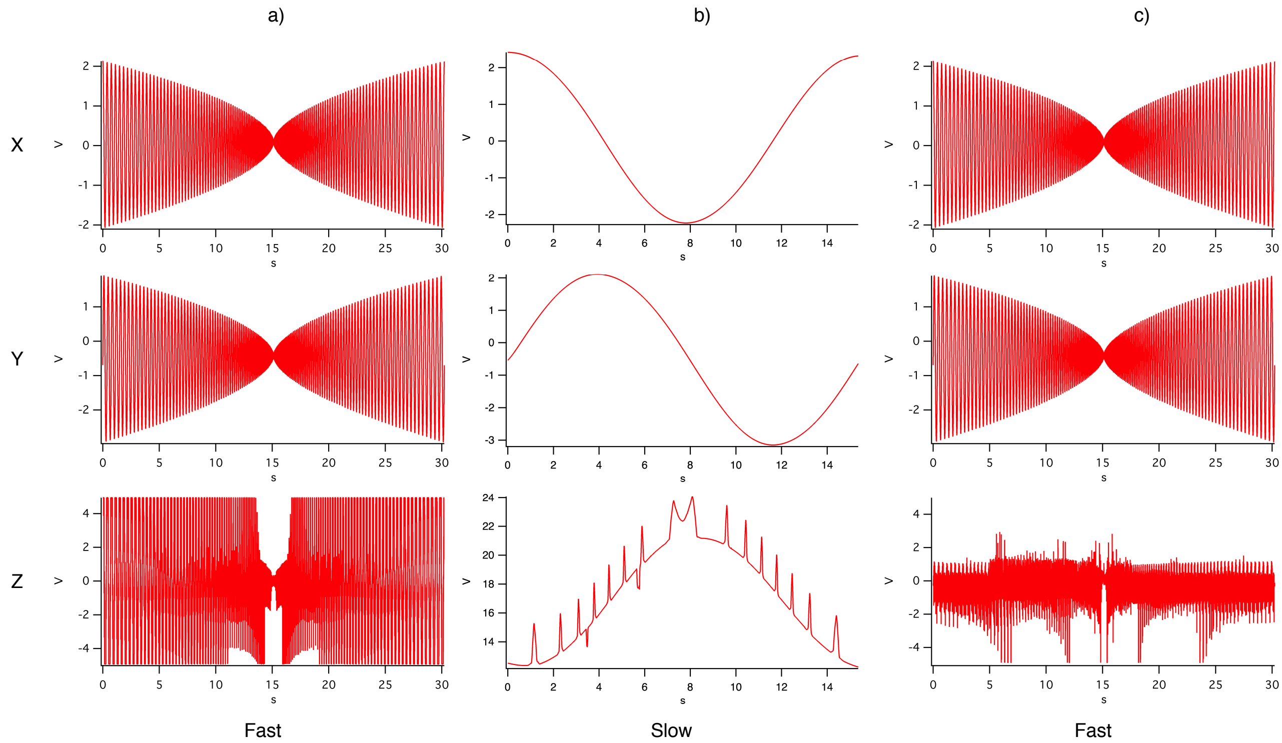

Figure 4.5: Path on the XY plane

a_1	a_2	a_3
-0.14615	-0.031882	29.537

Table 4.1: Planefit coefficients

The figure 4.6 shows the wave we are going to send to the microscope. The x,y values of the wave's equation (3.2) are the output values of the scan pattern.

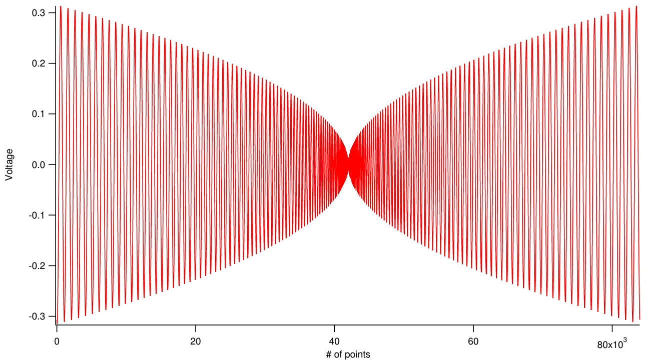

Figure 4.6: Input of the tilt compensation

We have calibrated the small piezoelectric ceramic and found that a step of 5V is equal to 90 nm (range of the piezo).

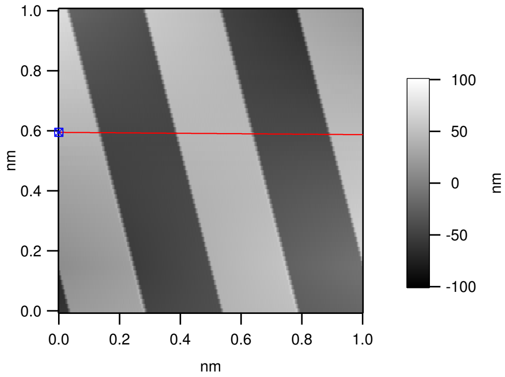

Figure 4.7: Height of the calibration

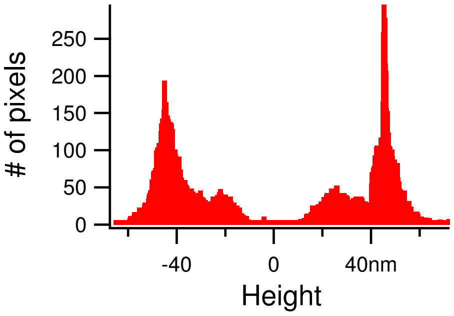

Figure 4.8: Histogram of the calibration

The tilt compensation takes a load off the small fast piezoelectrical ceramics. The Figure 4.9 shows the efficiency of our method. Indeed, the fast piezo was previously saturating. The piezo was trying to reach features that are larger than its range. If we use the tilt correction, we see that our piezo has no problem reaching those features.

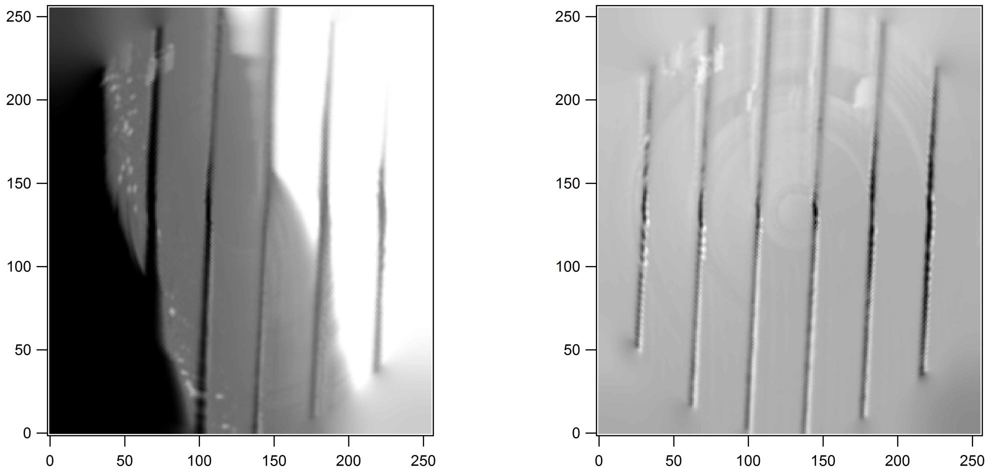

Figure 4.9: Before and after the tilt correction

5 Conclusion

In this thesis, we saw different methods to improve AFM bandwidth and speed on the X,Y,Z axis.

In the first part, we have discussed using spiral patterns instead of raster one. We have taken another approach and decided to use the data of the position sensors on the X,Y axis instead of steering the tip on specific position of the grid. Then, we have implemented advanced image processing algorithms to render images from the sparse data. We have shown that programming vertex buffer objects improve the performances of the rendering. Moreover, heat equations inpainting is a powerful tool to fill missing spots of an image.

In the second part, we have investigated new ways to compensate for inaccuracies on the z-axis. Indeed, we have designed an algorithm to measure the tilt of a sample and dynamically compensate for it. Also, we have implemented a dual actuators system. This system has an additional high bandwidth piezoelectrical ceramic that can measure small features of the surface. When we use the dual actuator system and the small piezoelectrical ceramic, we can achieve higher bandwidth while keep the same amplitude range.

Finally, we have designed two experiments to test our new implementations(tilt correction and dual actuator feedback). Our correction algorithm successfully compensated the tilt on the surface of a calibration grating. Also, we have imaged calcite dissolution with the dual actuator feedback. Future research should leverage these techniques to perform high speed scanning on more samples.

Arnaud Benard, 03.13.2013

A Programming

A.1 Structure of the Spiral Scan program

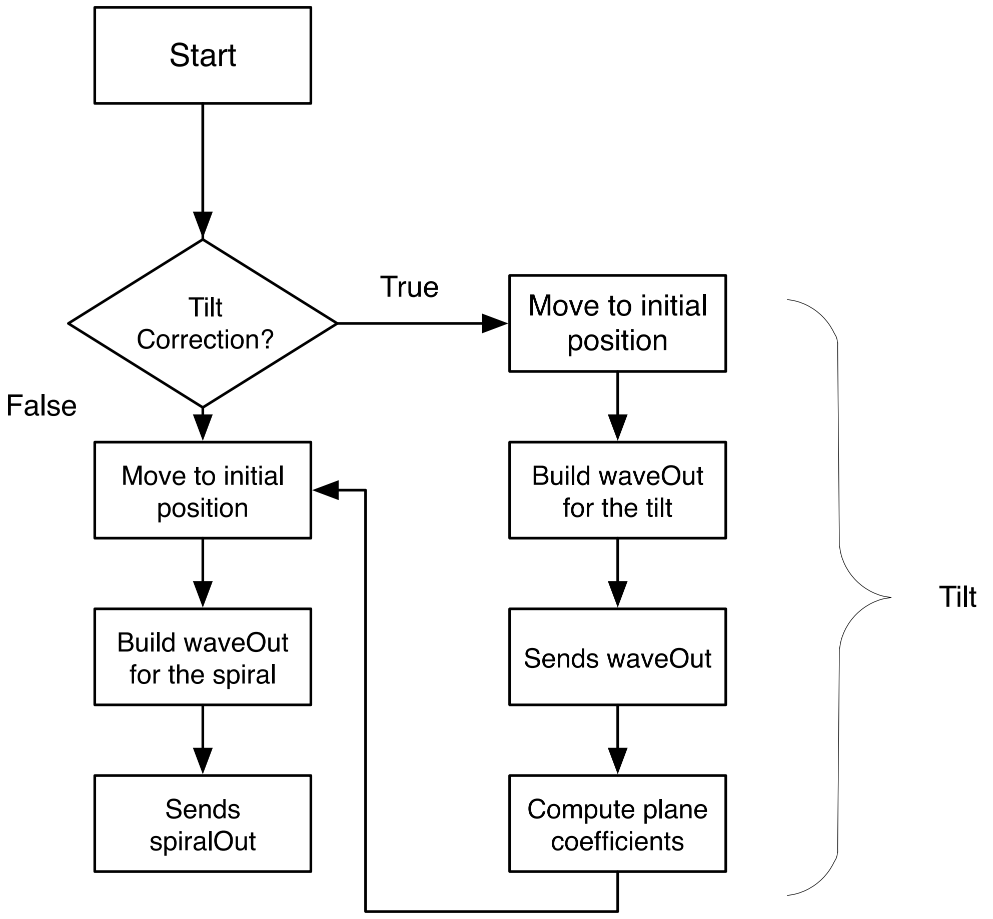

Figure A.1: Flowchart of the spiral scanning program

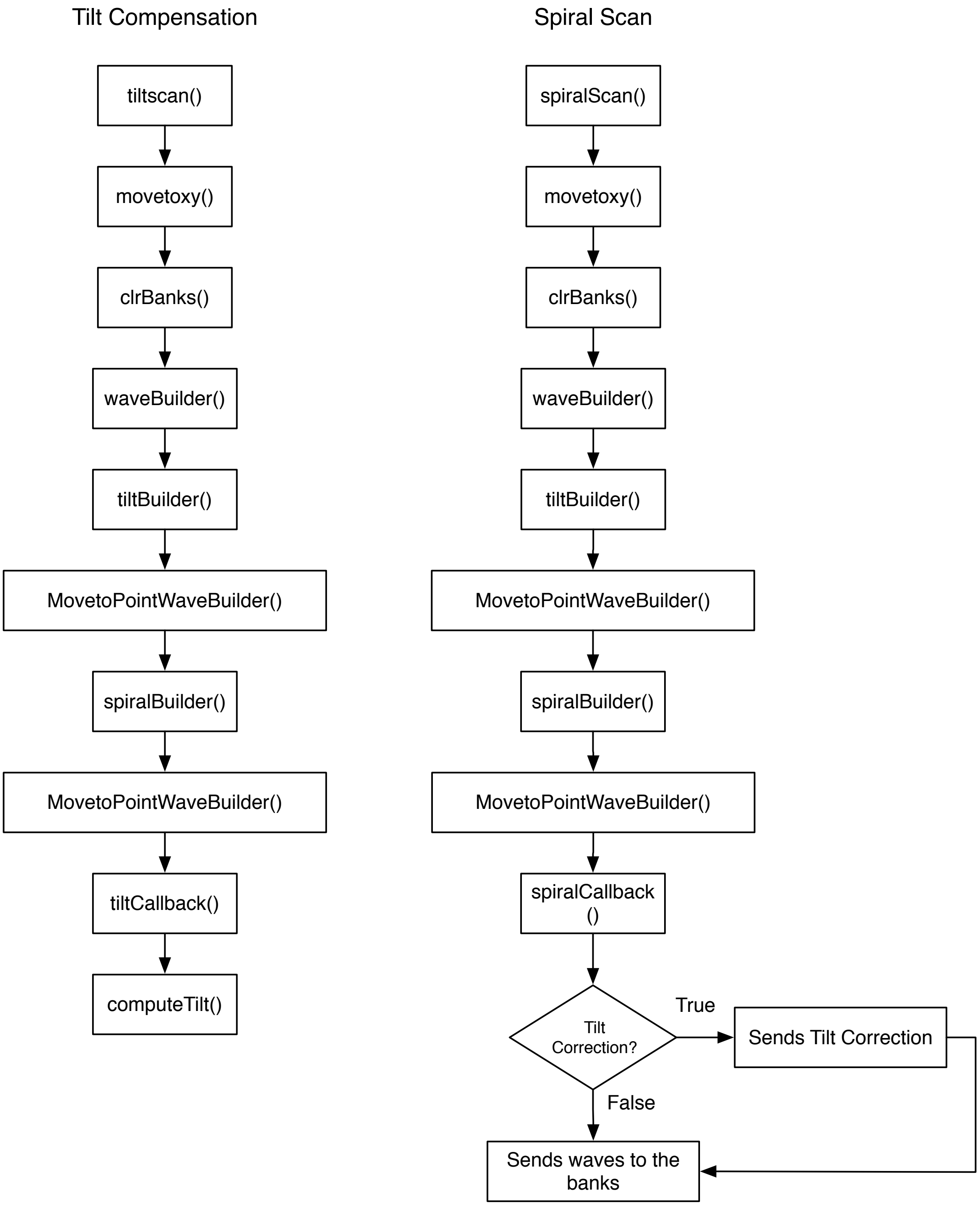

Figure A.2: Function call of the spiral scanning program

A.2 User interface Igor Pro

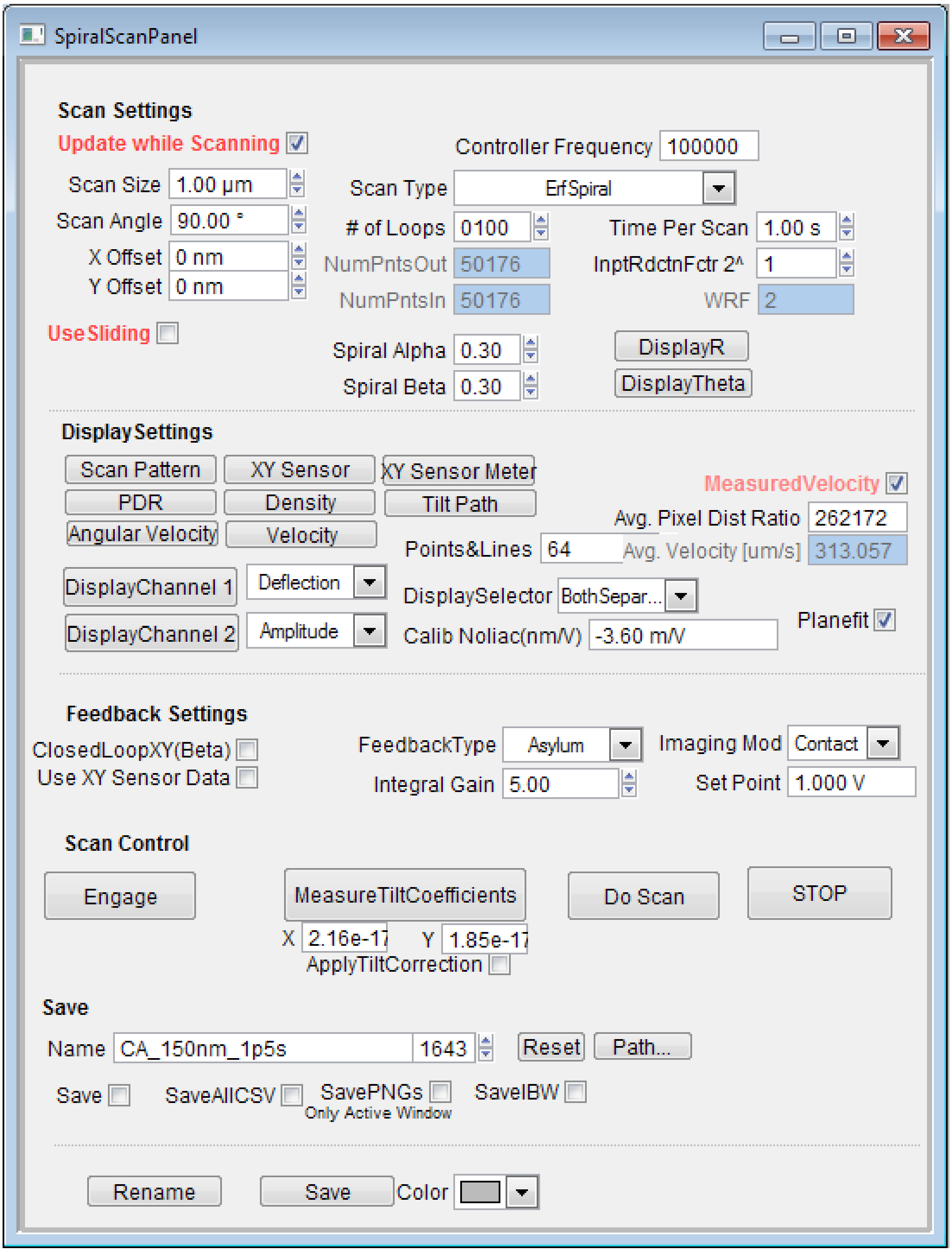

SpiralScanPanel

Scan Settings

Update while Scanning ☑

Controller Frequency 100000

Scan Size 1.00 µm

Scan Angle 90.00 °

X Offset 0 nm

Y Offset 0 nm

Use Sliding □

Scan Type ErfSpiral

# of Loops 0100

NumPntsOut 50176

NumPntsIn 50176

Time Per Scan 1.00 s

InptRdctnFctr 2^ 1

WRF 2

Spiral Alpha 0.30

Spiral Beta 0.30

Display Settings

MeasuredVelocity ☑

Avg. Pixel Dist Ratio 262172

Points&Lines 64

Avg. Velocity [um/s] 313.057

DisplayChannel 1 Deflection

DisplayChannel 2 Amplitude

DisplaySelector BothSepar...

Calib Noliac(nm/V) -3.60 m/V

Planefit ☑

Feedback Settings

ClosedLoopXY(Beta) □

Use XY Sensor Data □

FeedbackType Asylum

Integral Gain 5.00

Imaging Mod Contact

Set Point 1.000 V

Scan Control

X 2.16e-17 Y 1.85e-17

ApplyTiltCorrection □

Save

Name CA_150nm_1p5s 1643

Save □ SaveAllCSV □ SavePNGs □ Only Active Window SaveIBW □

Figure A.3: User interface spiral scanning

A.3 Other figures

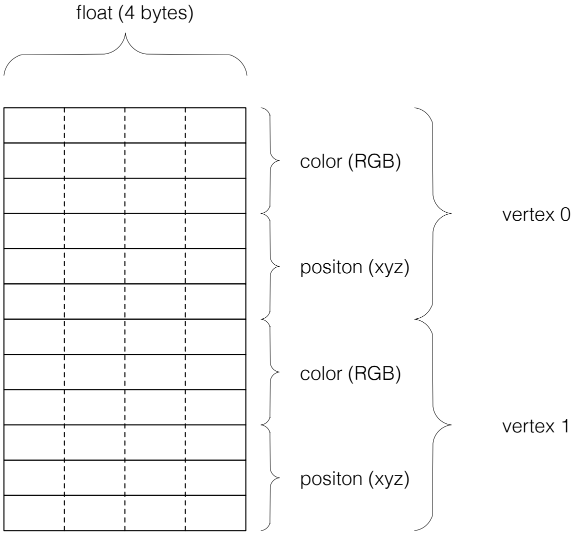

Figure A.4: Memory for the VAO

Bibliography

[1] Asylum research. Mfp-3d stand alone atomic force microscope from asylum research. 2013.

[2] Yaldex. Server-side vertex arrays. 2013.

[3] Gerd Binnig, Calvin F Quate, and Ch Gerber. Atomic force microscope. *Physical review letters*, 56(9):930–933, 1986.

[4] Manfred Radmacher. Measuring the elastic properties of biological samples with the afm. *Engineering in Medicine and Biology Magazine, IEEE*, 16(2):47–57, 1997.

[5] PK Hansma, VB Elings, O Marti, CE Bracker, et al. Scanning tunneling microscopy and atomic force microscopy: application to biology and technology. *Science (New York, NY)*, 242(4876):209, 1988.

[6] YK Yong, SOR Moheimani, and IR Petersen. High-speed cycloid-scan atomic force microscopy. *Nanotechnology*, 21(36):365503, 2010.

[7] IA Mahmood and SO Reza Moheimani. Fast spiral-scan atomic force microscopy. *Nanotechnology*, 20(36):365503, 2009.

[8] Peng Huang and S.B. Andersson. Generating images from non-raster data in afm. In *American Control Conference (ACC), 2011*, pages 2246 –2251, 29 2011-july 1 2011.

[9] Manuel M Oliveira Brian Bowen Richard and McKenna Yu-Sung Chang. Fast digital image inpainting. In *Appeared in the Proceedings of the International Conference on Visualization, Imaging and Image Processing (VIIP 2001), Marbella, Spain*, 2001.

[10] Younkoo Jeong, G. R. Jayanth, and Chia-Hsiang Menq. Control of tip-to-sample distance in atomic force microscopy: A dual-actuator tip-motion control scheme. *Review of Scientific Instruments*, 78(9):093706, 2007.

[11] T Sulchek, SC Minne, JD Adams, DA Fletcher, A Atalar, CF Quate, and DM Adderton. Dual integrated actuators for extended range high speed atomic force microscopy. *Applied physics letters*, 75(11):1637–1639, 1999.

[12] Gilles Aubert and Pierre Kornprobst. *Mathematical problems in image processing: partial differential equations and the calculus of variations*, volume 147. Springer, 2006.

[13] Abobe. Tips for optimizing gpu rendering performance. 2013.

[14] Jonathan Richard Shewchuk. Triangle: Engineering a 2D Quality Mesh Generator and Delaunay Triangulator. In Ming C. Lin and Dinesh Manocha, editors, *Applied Computational Geometry: Towards Geometric Engineering*, volume 1148 of *Lecture Notes in Computer Science*, pages 203–222. Springer-Verlag, May 1996. From the First ACM Workshop on Applied Computational Geometry.

[15] Mark J. Kilgard. Modern opengl usage: Using vertex buffer objects well. Technical report, 2008.

[16] OpenGL, 2012.

[17] Khalid El Rifai, Osamah El Rifai, and Kamal Youcef-Toumi. On dual actuation in atomic force microscopes. In *American Control Conference, 2004. Proceedings of the 2004*, volume 4, pages 3128–3133. IEEE, 2004.

[18] PE Hillner, AJ Gratz, S Manne, and PK Hansma. Atomic-scale imaging of calcite growth and dissolution in real time. *Geology*, 20(4):359–362, 1992.

[19] Yong Liang, Donald R Baer, James M McCoy, James E Amonette, and John P Lafemina. Dissolution kinetics at the calcite-water interface. *Geochimica et Cosmochimica Acta*, 60(23):4883–4887, 1996.

[20] Jeanne Paquette and Richard J Reeder. Relationship between surface structure, growth mechanism, and trace element incorporation in calcite. *Geochimica et Cosmochimica Acta*, 59(4):735–749, 1995.

[21] Ryoji Shiraki, Peter A Rock, and William H Casey. Dissolution kinetics of calcite in 0.1 m nacl solution at room temperature: An atomic force microscopic (afm) study. *Aquatic Geochemistry*, 6(1):87–108, 2000.

[22] John W Morse and Rolf S Arvidson. The dissolution kinetics of major sedimentary carbonate minerals. *Earth-Science Reviews*, 58(1â€“2):51 – 84, 2002.